Comparison of Methods for Modeling Uncertainties in a 2D Hyperthermia Problem

Damien Voyer, François Musy, Laurent Nicolas, Ronan Perrussel

Impact of uncertainties in 2D hyperthermia using stochastic spectral and collocation methods

Damien Voyer⋆, François Musy†, Laurent Nicolas⋆ and Ronan Perrussel⋆
⋆ Laboratoire Ampère (UMR CNRS 5005), Université de Lyon, École Centrale de Lyon, Écully, France
† Institut Camille Jordan (UMR CNRS 5208), Université de Lyon, École Centrale de Lyon, Écully, France
Damien.Voyer@ec-lyon.fr

***Abstract*—Uncertainties in biological tissue properties are weighed in the case of an hyperthermia calculation. Stochastic spectral and collocation methods are applied to analyze the impact of these uncertainties on the distribution of the electromagnetic power absorbed inside the body of a patient. They enable to realize sensitivity and uncertainty analyses more efficiently than when using a two level experimental design or a kriging technique.**

***Index Terms*—stochastic method, adaptive sparse grid, numerical dosimetry**

I. Introduction

AN IMPORTANT issue in hyperthermia and more generally in numerical dosimetry tackles the variability of the biological tissue properties [1]. This variability can be modeled by considering those properties as *random variables* with probabilistic laws in agreement with the existing experimental data. The problem consists then in evaluating how this alea affects physical quantities such as the distribution of the electromagnetic power absorbed inside the human body. In this paper, some variability is introduced in the different tissues of a 2D hyperthermia problem. In order to determine the *most influential factors* and *quantify* their effects, different approaches are briefly presented and compared in terms of accuracy and computational cost: a two level experimental design approach [2], kriging approach [3] and finally, stochastic spectral [4] and collocation [5] methods using adaptive sparse grid [6].

II. Hyperthermia problem

It is considered the treatment of a tumor located inside the liver of a patient. The 2D model has been obtained from a computed tomography slice of the body.

In a *first step*, the electromagnetic properties – permittivity ϵ and conductivity σ – of the different tissues are set to the common values used in literature [7] (see Table I). The amplitudes and the phases of four incident waves are adjusted so that to maximize the power absorbed inside the liver and minimize the power absorbed elsewhere in the body. More precisely, the quantity we minimize is:

$$y = \frac{\int_{\text{body} \neq \text{liver}} \sigma(\tau) |E(\tau)|^2 d\tau}{\int_{\text{liver}} \sigma(\tau) |E(\tau)|^2 d\tau} \quad (1)$$

where E is the amplitude of the electric field. Computations are performed using the finite element library getfem++ [8].

In a *second step*, the properties of the different tissues are supposed to be random variables with uniform probability laws while the phases and amplitudes of the four incident waves found are maintained at the values found at the first step. The properties of the tissues vary in a range of $\pm 25\%$ around the mean value except those of the tumor which vary in a range of $\pm 50\%$; this distinction is introduced because the properties of tumors are usually less known than those of safe tissues.

TABLE I
Mean values of tissue parameters involved in the hyperthermia problem and range of variation

Quantity	Mean	Variation
σ muscle	0.707	$\pm 25\%$
ϵ_r muscle	65.972	$\pm 25\%$
σ fluid body	1.504	$\pm 25\%$
ϵ_r fluid body	69.085	$\pm 25\%$
σ bone	0.064	$\pm 25\%$
ϵ_r bone	15.283	$\pm 25\%$
σ marrow	0.022	$\pm 25\%$
ϵ_r marrow	6.488	$\pm 25\%$
σ kidney	0.810	$\pm 25\%$
ϵ_r kidney	98.094	$\pm 25\%$
σ liver	0.487	$\pm 25\%$
ϵ_r liver	69.022	$\pm 25\%$
σ tumor	1.005	$\pm \mathbf{50}\%$
ϵ_r tumor	84.342	$\pm \mathbf{50}\%$
σ bowel	1.655	$\pm 25\%$
ϵ_r bowel	96.549	$\pm 25\%$
σ lung	0.558	$\pm 25\%$
ϵ_r lung	67.108	$\pm 25\%$

In the following, y defined in (1) is the observed quantity; it is a random variable depending on the 18 random variables corresponding to the tissue properties. For each of the strategies mentioned in the Introduction, a *specific model* for y is assumed and a *specific numerical experimental design* is built in order to estimate the unknown parameters of the model. Such a design consists in the choice of a set of realizations or *nodes* for the random variables. Comparisons are proposed in terms of sensitivity and uncertainty analyses.

III. Classic two level experimental design

The random input variables are normalized between -1, the low level, and $+1$, the high level. The model for y is:

$$y(\widetilde{\boldsymbol{x}}) = \beta_0 + \sum_{i=1}^{18} \beta_i \widetilde{x}_i + \sum_{i=1}^{18} \sum_{j>i} \beta_{i,j} \widetilde{x}_i \widetilde{x}_j + \cdots + \epsilon(\widetilde{\boldsymbol{x}}) \quad (2)$$

where $\widetilde{\boldsymbol{x}} = \{\widetilde{x}_i\}_{i=1,\ldots,18} \in [-1,1]^{18}$ denote the normalized variables. The coefficients $\{\beta_i\}_{i=1,\ldots,18}$ correspond to the main components, $\{\beta_{i,j}\}_{i,j=1,\ldots,18;\ j>i}$ correspond to the interactions between two variables; higher order interactions are also considered. The first part of the model is the *regression model* and the remaining ϵ is the *error*. This error is supposed to be a random process with a zero mean and where *two realizations are uncorrelated*.

Once a numeric experimental design is built, the estimate $\widehat{\beta}$ of β is the *ordinary least square solution* based on the nodes of the design. In statistics, it is also the *best linear unbiased predictor* for β.

In a *two level experimental design*, the nodes are chosen at the edges of the domain and thus each $\tilde{x}_i$ can take the values -1 and $+1$. Consequently, the complete design will involve $2^{18} = 262,144$ nodes. When the numerical experiments are expensive in computational resources, the complete design cannot be realized. A solution is to consider fractional experimental designs where some effects are confounded. A fractional design is characterized by its resolution: in a resolution III, main components can be confounded with interactions of order 2; in a resolution IV, main components cannot be confounded with interactions of order 2 but two interactions of order 2 can be confounded.

TABLE II
Results for the fractional experimental design

Quantity	Coefficient	Resolution III 2^{18-13} 32 nodes	Resolution IV 2^{18-12} 64 nodes
	β_0	16.888	17.194
σ muscle	β_1	3.378	2.514
ϵ_r muscle	β_2	-1.222	-2.0237
σ fluid body	β_3	**5.976**	**6.812**
ϵ_r fluid body	β_4	**-5.348**	**-5.485**
σ bone	β_5	1.035	0.845
ϵ_r bone	β_6	-0.796	0.508
σ marrow	β_7	0.331	-0.538
ϵ_r marrow	β_8	-0.485	0.297
σ kidney	β_9	0.150	-0.309
ϵ_r kidney	β_{10}	0.124	0.231
σ liver	β_{11}	**-5.421**	**-5.935**
ϵ_r liver	β_{12}	**4.679**	**4.930**
σ tumor	β_{13}	-1.812	-1.689
ϵ_r tumor	β_{14}	-1.565	1.322
σ bowel	β_{15}	-0.408	-0.249
ϵ_r bowel	β_{16}	0.179	-0.409
σ lung	β_{17}	-0.215	-0.120
ϵ_r lung	β_{18}	0.530	0.119

Fractional designs of resolution III and IV have been applied to the hyperthermia problem. The results are detailed in Table II. Our attention is focused on the most influential components even though an experimental design enables to extract also information on the interactions between factors. As the quality of the resolution increases, the cost also increases: 32 nodes for a resolution III and 64 nodes for a resolution IV. It appears that *the properties of the liver and the fluid body have the greatest influence* on the value of y; the properties of the muscle have a lower impact. As shown in the next sections, these results are in agreement with those obtained by other methods. On the other hand, they give little importance to the properties of the tumor and the bone, which is actually unexpected. Moreover, there is a discrepancy in the estimation of the coefficients β_6 and β_{14} between resolution III and IV. In order to refine the results, the resolution should be increased but the numerical cost will also strongly increase: 512 nodes is required for the resolution VI – resolution V does not exist for this example –.

IV. Kriging

In the kriging approach, the model of y is composed of a regression model, as in classic experimental design, and of an error whose properties are different from the error given in (2). Indeed, the error is chosen to be a stationary gaussian process with a zero mean but where *two realizations are correlated*. From the numeric experimental design, the parameters of the correlation function are estimated and it enables to correct the systematic bias that appears between y and the regression model at the nodes of the design.

The software *GEM-SA* [9] is used to test the kriging method. To compute the model of y, it generates a *Latin hypercube design* of the initial hypercube with 18 dimensions. For a user-defined number of nodes, this Latin hypercube is the result of an optimization process of the *space-filling properties*.

TABLE III
Results for the kriging approach: partial variance (%) and total effect (%) of the different parameters

Quantity	40 nodes		100 nodes	
	Variance	Effect	Variance	Effect
σ muscle	2.40	2.79	2.14	2.35
ϵ_r muscle	2.82	3.59	1.25	1.51
σ fluid body	**29.26**	**34.25**	**27.06**	**31.86**
ϵ_r fluid body	**17.56**	**21.72**	**19.90**	**24.74**
σ bone	0.20	0.28	0.01	0.05
ϵ_r bone	0.14	0.14	0.02	0.05
σ marrow	0.44	0.51	0.04	0.04
ϵ_r marrow	0.05	0.25	0.03	0.07
σ kidney	0.24	0.24	0.01	0.01
ϵ_r kidney	0.14	0.25	0.03	0.04
σ liver	**20.02**	**22.17**	**22.85**	**25.91**
ϵ_r liver	**18.00**	**19.15**	**17.77**	**19.87**
σ tumor	0.59	0.75	0.16	0.41
ϵ_r tumor	0.29	0.29	0.25	0.87
σ bowel	0.49	0.62	0.04	0.49
ϵ_r bowel	0.13	0.13	0.03	0.24
σ lung	0.11	0.14	0.04	0.35
ϵ_r lung	0.09	0.09	0.04	0.17

Two simulations of the hyperthermia problem have been carried out using 40 nodes and 100 nodes. The sensitivity analysis is given in Table III: for each input random variable x_i, the partial variance, which corresponds to $\mathrm{Var}[\mathrm{E}[y|x_i]]/\mathrm{Var}[y]$ where $\mathrm{E}[\cdot]$ denotes the expectancy, and the total effect, which adds to the partial variance the contribution to the variance of the higher order interactions involving x_i [10], are computed.

It appears that *the properties of the fluid body and the liver are the most influential parameters* on y. The muscle also has an effect but less important. The other variables do not have any influence on y. In particular, the contribution of the tumor is insignificant: this is due to the fact that the tumor is small and consequently, its influence on the integral in (1) is negligible. Moreover, it seems that there is *low coupling* between the different variables since *the partial variance is close to the total effect*. As for the mean and the variance, the results are in accordance with those obtained in the next sections (see Table IV).

TABLE IV
MEAN AND VARIANCE COMPUTED USING THE DIFFERENT APPROACHES

Method	Kriging		Stochastic spectral method		Stochastic collocation method	
Number of nodes	40	100	150	1 000	160	1 000
Mean	14.082	14.218	14.138	14.131	14.131	14.135
Variance	41.558	42.518	40.140	40.341	39.786	40.846

V. STOCHASTIC SPECTRAL METHOD

The stochastic spectral method is based on the expansion of the random variable y in a polynomial basis depending on the input random variables. Since the input random variables are characterized by uniform laws, it can be efficiently expanded on the generalized polynomial chaos [11] based on the Legendre polynomials:

$$y(\boldsymbol{\xi}) = \sum_{\mathbf{i}\in\mathbb{N}^{18}} y_{\mathbf{i}} \Psi_{\mathbf{i}}(\boldsymbol{\xi}) \tag{3}$$

where $\Psi_{\mathbf{i}}(\boldsymbol{\xi}) = \prod_{j=1}^{18} L_{g\,i_j}(\xi_j)$; $L_{g\,k}$ are the Legendre polynomials and $\boldsymbol{\xi} = \{\xi_i\}_{i=1,\ldots,18}$ the normalized input random variables with uniform laws defined on $[-1,1]$. The *total degree* of the polynomial is the sum of the indexes i_j.

The unknown coefficients $y_{\mathbf{i}}$ in (3) can be computed using the projection method:

$$y_{\mathbf{i}} = \frac{\mathrm{E}[y\Psi_{\mathbf{i}}]}{\mathrm{E}[\Psi_{\mathbf{i}}^2]} = \frac{1}{\prod_{j=1}^{18} i_j!} \int_{[-1,\,1]^{18}} y(\boldsymbol{\xi})\,\Psi_{\mathbf{i}}(\boldsymbol{\xi})\,\frac{1}{2^{18}} d\boldsymbol{\xi}, \tag{4}$$

To compute the integral in (4), quadrature rules are applied and define the numerical experimental design. This *scientific computing approach* is quite different from the *statistic approach* using Latin hypercubes discussed in the previous section. However, applying a tensor product design based on one-dimensional Gaussian quadrature rules is most of the time prohibitive since the number of quadrature nodes increases exponentially with the number of dimensions. For instance, an exact integration up to the order 7 requires $4^{18} = 68,719,476,736$ simulations. This number can be dramatically reduced using *sparse grid*: only $9,841$ have to be computed when considering Smolyak's algorithm with *Gauss Patterson nodes*. Nonetheless, an *adaptive sparse grid algorithm* is even more suited in order to explore only the most influential factors. This technique is used with Gauss Patterson nodes since their building relies on *nested sequences of nodes* at the different levels of accuracy [6].

Our criterion for adaptivity in the hyperthermia problem is based on the variance. From (3), the variance is given by:

$$\sigma_y^2 = \sum_{\mathbf{i}\in\mathbb{N}^{18}\setminus(0,\ldots,0)} y_{\mathbf{i}}^2. \tag{5}$$

In the adaptive version of Smolyak's algorithm, a comparison of the increment of variance brought by each direction provides the error indicator allowing to choose in which direction the accuracy of the quadrature has to be increased. A direction in the algorithm is described by the index $\mathbf{i} = [i_1, \ldots, i_{18}]$ where the component i_j indicates a level of accuracy of the quadrature rule following the j-th variable. In (5), the sum is reduced to the indexes $\mathbf{i}$ for which the numerical integration of $\mathrm{E}[\Psi_{\mathbf{i}}^2]$ is exact. At the beginning of the algorithm, only one point is computed and it corresponds to the index $[0,\ldots,0]$. At this stage, only the term y_0 can be estimated and no term is available to calculate the variance in (5). At the first iteration of Smolyak's algorithm, the level of accuracy is increased successively for each variable *i.e.* from index $[1,0,0,\ldots,0]$ to $[0,0,\ldots,0,1]$. At this step, only the coefficients related to the polynomials of total degree less or equal to 1 are calculated from (4). Then, the variance in (5) is reduced to a sum of 18 terms. At the second iteration of Smolyak's algorithm, the level of accuracy is increased from the direction that has brought the largest contribution to the variance. The new sequences are used to refine the calculation of existing $y_{\mathbf{i}}$ coefficients but also to integrate new $y_{\mathbf{i}}$ coefficients that can be computed more precisely with the new nodes. This approach can be seen as an adaptive building of the polynomial chaos.

Fig. 1 shows the convergence study of the stochastic spectral method. Two criteria have been experimented in the adaptive algorithm: first, only the contribution of an index to the variance is considered; second, the contribution of an index to the variance is balanced by the number of new nodes to calculate, *i.e.* the computing time cost of the new nodes is taken into account. It appears that the convergence is better when using the balanced variance criterion: in this case, the variance converges after about 150 nodes while it needs more than 400 nodes in the case of the unbalanced criterion. The variance converges to a value close to the result obtained with the kriging technique (see Table IV). However, the stochastic method gives a more accurate result with about one hundred nodes than the kriging method.

The sensitivity analysis is reported in Table V: the data are in agreement with those obtained by the kriging method. Three tissues impact on the variability of y: the fluid body, the liver and the muscle. The others are nearly negligible and their influence is more residual than in the kriging prediction.

VI. STOCHASTIC COLLOCATION METHOD

Sparse grid with an adaptive algorithm can also be exploited to interpolate y. In this case, the interpolation function is obtained using multi-dimensional Lagrange's polynomials. As

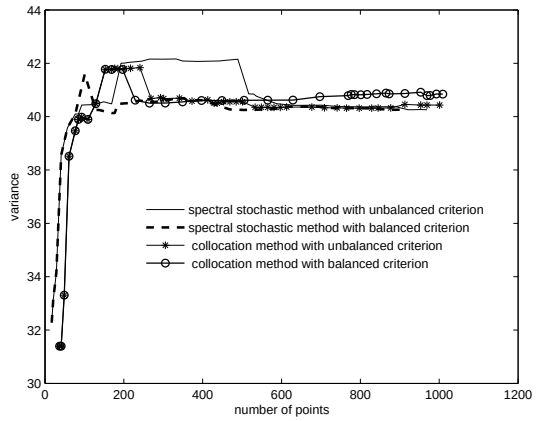

Fig. 1. Convergence of the stochastic spectral and collocation methods using an unbalanced criterion and a balanced one.

TABLE V
RESULTS FOR STOCHASTIC SPECTRAL METHOD: PARTIAL VARIANCE (%) AND TOTAL EFFECT (%) OF THE DIFFERENT PARAMETERS

Quantity	150 nodes		1000 nodes	
	Variance	Effect	Variance	Effect
σ muscle	2.80	3.20	2.79	3.29
ϵ_r muscle	1.82	2.16	1.80	2.16
σ fluid body	**28.19**	**32.34**	**27.86**	**32.50**
ϵ_r fluid body	**19.88**	**23.50**	**19.58**	**23.54**
σ bone	0.00	0.00	0.00	0.00
ϵ_r bone	0.00	0.00	0.00	0.00
σ marrow	0.00	0.00	0.00	0.00
ϵ_r marrow	0.00	0.00	0.00	0.00
σ kidney	0.00	0.00	0.00	0.00
ϵ_r kidney	0.00	0.00	0.00	0.00
σ liver	**23.89**	**26.60**	**23.67**	**26.78**
ϵ_r liver	**16.12**	**17.91**	**15.89**	**18.00**
σ tumor	0.10	0.10	0.28	0.50
ϵ_r tumor	0.52	0.67	0.50	0.89
σ bowel	0.02	0.02	0.03	0.03
ϵ_r bowel	0.03	0.03	0.04	0.04
σ lung	0.00	0.00	0.00	0.00
ϵ_r lung	0.00	0.00	0.00	0.00

the sequences of Gauss Patterson nodes are nested, when the value of y is computed on new nodes, the error indicator is given by the absolute difference with the values interpolated using the older nodes.

In this section, we use the matlab *sparse grid interpolation toolbox* [12]. As in the previous section, the adaptivity criterion can or cannot be balanced by the numerical cost of a sequence. Both situations have been carried out and the results are given in Fig. 1. It appears that the results do not converge exactly to the same value: with $1\,000$ nodes, $\sigma_y^2 = 40.434$ for the unbalanced criterion whereas $\sigma_y^2 = 40.846$ for the balanced one. The result with the unbalanced criterion is closer to the result given by the stochastic spectral method. Moreover, it seems that the convergence is achieved later compared to the stochastic spectral method. This could be due to the fact that the collocation method adaptivity is related to the quality of the interpolation whereas the spectral method adaptivity is directly linked to the variance. The effect of the different strategies can also be viewed when one is interested in the maximum polynomial order reached in the 18 variables. Fig. 2 shows this result after $1\,000$ nodes for the spectral method and the collocation method. In both case, the most influential variables – 1, 2, 3, 4, 11 and 12 – are largely explored. The variables associated to the tumor properties – 13 and 14 – are also exploited because of their weaker but existing influence. However, the collocation method goes further in the exploration of the variable 16 that corresponds to the bowel permittivity but this variable does not contribute to the variance as shown in Tables III and V. Finally, the mean results are

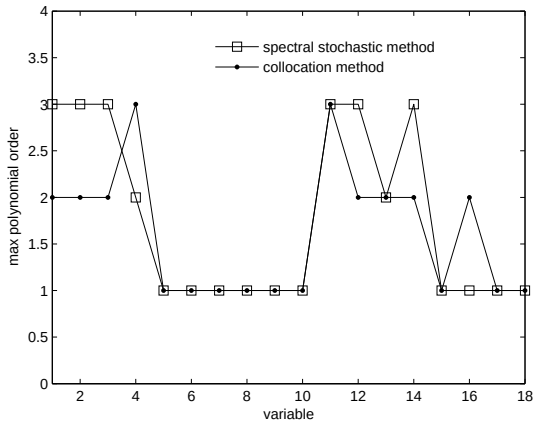

Fig. 2. Maximum order polynomial reached in each variable for the stochastic spectral and collocation methods.

similar to the ones given by the spectral method (see Table IV).

VII. CONCLUSION

The presence of uncertainties in the tissue properties has been analyzed in a 2D hyperthermia problem. Among the 18 uncertain properties, only those related to the tissues located in the neighborhood of the tumor have an impact on the repartition of absorbed power. The sensitivity analysis made with fractional experimental design leads to erroneous conclusions; the sensitivity and uncertainty analyses using the kriging technique give more accurate results. However, it appears that the spectral stochastic method using an adaptive sparse grid algorithm is optimal in this problem: convergence is reached with about one hundred nodes. Using an adaptive sparse grid algorithm in a stochastic collocation method is less efficient in this case.

REFERENCES

[1] W. D. Hurt, J. M. Ziriax, and P. A. Mason, "Variability in EMF permittivity values: implications for SAR calculations," *Biomedical Engineering, IEEE Trans. on*, vol. 47, no. 3, pp. 396–401, March 2000.
[2] A. Garcia-Diaz and D. Philips, *Principles of experimental design and analysis*. Chapman & Hall, 1995.
[3] J. Koehler and A. Owen, *Handbook of statistics*. Elsevier Science, 1996, ch. Computer experiments, pp. 261–308.
[4] R. G. Ghanem and P. D. Spanos, *Stochastic finite elements: a spectral approach*. New York: Springer-Verlag, 1991.
[5] D. Xiu and J. S. Hesthaven, "High-order collocation methods for differential equations with random inputs," *SIAM Journal on Scientific Computing*, vol. 27, no. 3, pp. 1118–1139, 2005.

[6] T. Gerstner and M. Griebel, "Dimension-adaptive tensor-product quadrature," *Computing, Springer-Verlag New York, Inc.*, vol. 71, no. 1, pp. 65–87, 2003.
[7] IFAC, Institute For Applied Physics. http://niremf.ifac.cnr.it/tissprop/.
[8] Y. Renard and J. Pommier, Getfem finite element library. http://home.gna.org/getfem/.
[9] T. O'Hagan and M. Kennedy, Gaussian emulator machine software. http://www.tonyohagan.co.uk/academic/GEM/index.html.
[10] I. M. Sobol, "Sensitivity estimates for non linear mathematical models," *Mathematical Modelling and Computational Experiments*, vol. 1, pp. 407–414, 1993.
[11] D. Xiu and G. E. Karniadakis, "The Wiener-Askey polynomial chaos for stochastic differential equations," *SIAM J. Sci. Comput.*, vol. 24, no. 2, pp. 619–644 (electronic), 2002.
[12] A. Klimke, Sparse grid interpolation toolbox. http://www.ians.uni-stuttgart.de/spinterp/.